Electronic Supplementary Material (ESI) for RSC Advances.

Supporting Information for

Low Temperature Hydrothermal Synthesis of Battery Grade Lithium Iron Phosphate

Peter Benedek, Nils Wenzler, Maksym Yarema, Vanessa Wood*

Laboratory of Nanoelectronics, Department of Information Technology and Electrical Engineering, ETH Zurich, CH-8092 Zurich, Switzerland

* vwood@ethz.ch

A. Size distribution determination

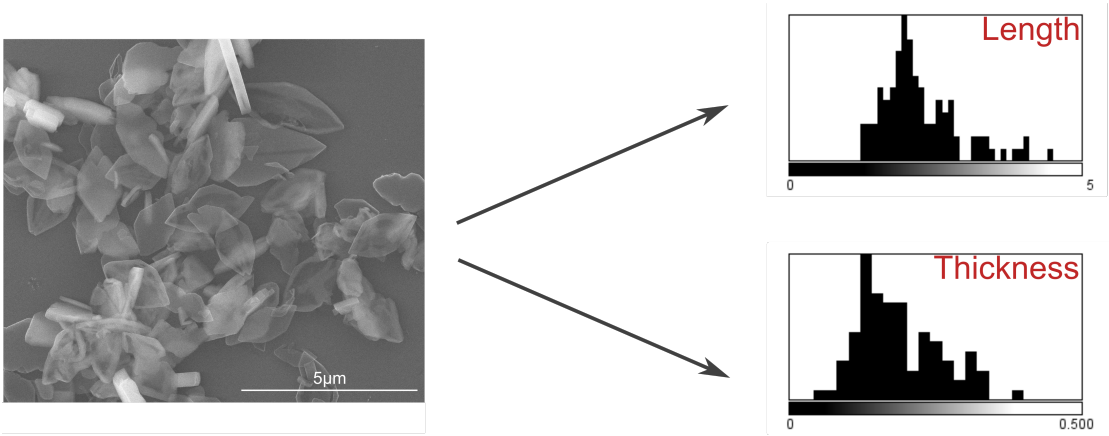

Figure 1S. Example size distributions for the LFP particles. The mean distance and the standard deviation of the particle length and thickness for each sample is obtained from the size distributions obtained by measuring 100-200 particles in multiple SEM images.

B. Carbon coating.

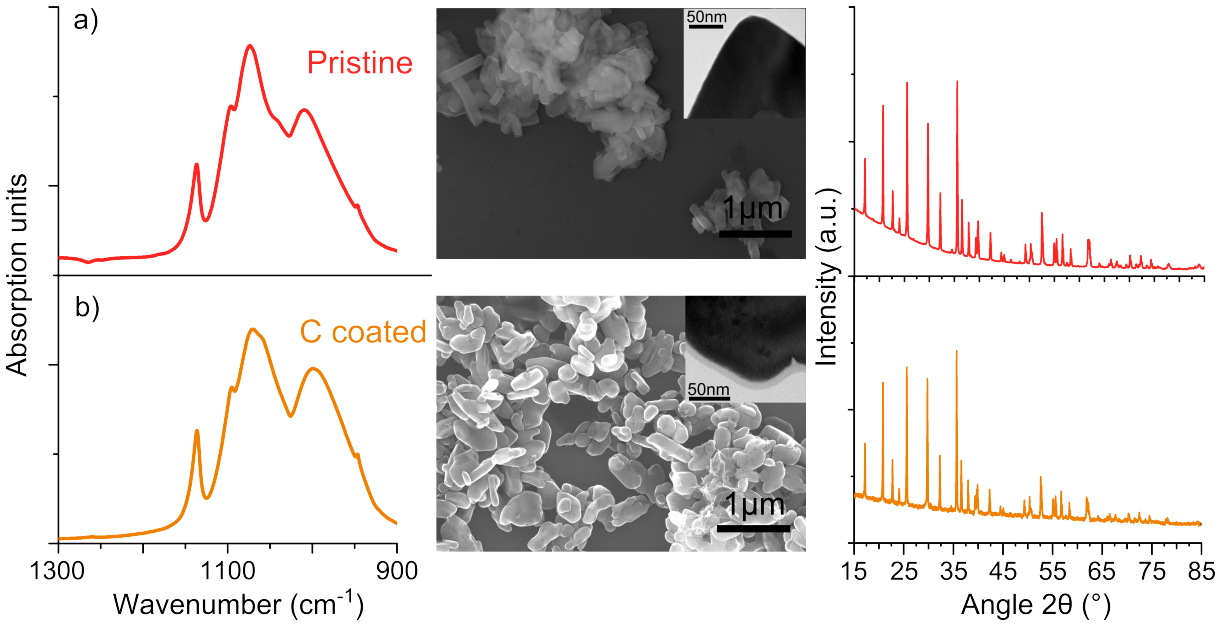

Figure 2S. Comparison of FTIR spectra, SEM and TEM images, and XRD patterns for LFP particles a) before and b) after annealing. The small change in the asymmetric PO_4 stretching mode likely comes from loss of water and some high temperature recrystallization during the annealing step. The XRD patterns show similar degrees of crystallization before and after annealing, indicating that no additional phases arise during the annealing.

C. Energy consumption analysis

We estimate the energy required for precursor production and synthesis of lithium iron phosphate (LFP) via a hydrothermal approach.

The energy consumption required for precursor production (per kg LFP) is calculated from different life cycle assessments[1-3] and is summarized in **Table 1S**. As iron (II) sulfate is a byproduct of the iron industry, the energy consumption for its production is neglected.

To estimate the energy consumption of the hydrothermal synthesis as a function of process parameters, we assume a hydrothermal reactor with a volume V = 10 m^3, a surface A = 25m^2 and an insulating wall with the thickness x = 0.1 m. Following the analysis of Majeau-Bettez[1] and Dunn[2], the total energy consumption per kg LFP is split into four terms,

$$\frac{E_{tot}}{m_{LFP}} = \frac{(E_{heat}+E_{loss})}{\eta_{tot}\, m_{LFP}} + E_{prec} - \frac{E_{rec}}{m_{LFP}}, \quad (1)$$

where E_{heat} is the energy required to heat the reactor, E_{loss} is the energy loss at the reactor walls, E_{prec} is the energy required to prepare the precursors per kg LFP, and E_{rec} is the energy recovered after the reaction, which we assumed to be half of the heating energy E_{heat}. The term η_{tot} is a product of reaction yield and the heater efficiency. To compare results, the total energy consumption is normalized to the LFP mass, produced per batch, m_{LFP}.

The energy loss through the wall is estimated with the conduction heat transfer equation (2), where λ is the heat exchange coefficient, t is the reaction time, and T_r, T_0 are the reactor and the ambient temperatures, respectively. Typical values are found in **Table 1S**.

$$E_{loss} = \frac{\lambda A(T_r - T_0)t}{x} \quad (2)$$

In contrast to previous work, here we model the energy consumption during reactor heating assuming that (1) the reactor is not completely filled and (2) water evaporates into the gas phase. These assumptions give a better estimate of the energy consumption than models where the entire liquid

volume is assumed to evaporate. This assumption is particularly important for low temperature syntheses, where only a small fraction of liquid converts to the vapor phase.

We define a filling factor, f, (see **Figure 3S**) and split the required heating energy in a vapor phase term E_{vap} and a liquid phase term E_{liq}. We assume that the liquid phase is incompressible and the volume change due to evaporation is negligible. Also, we assume ideal gas conditions of the gas phase and take the specific heat to be constant (e.g., neglect salt contributions in the liquid phase). We thus obtain:

$$E_{heat} = E_{vap} + E_{liq} \tag{3}$$

$$E_{vap} = m_{vap}\Delta_v H + \int_{T_0}^{T_f} m_{vap}(T) C_{vap}^{sp} \mathrm{d}T \tag{4}$$

$$E_{liq} = \int_{T_0}^{T_f} (m_{tot} - m_{vap}(T)) C_{liq}^{sp} \mathrm{d}T \tag{5}$$

$$m_{vap}(T) = \frac{M_{H_2O} p(T)(1-f)V}{RT} \tag{6}$$

where $\Delta_v H$ is the enthalpy of evaporation, m_{vap} is the mass of water in the vapor phase, C_i^{sp} is specific heat of the phase i, R is the universal gas constant, M_{H_20} is the molar mass of water, and $p(T)$ is the temperature dependent vapor pressure.[4,5]

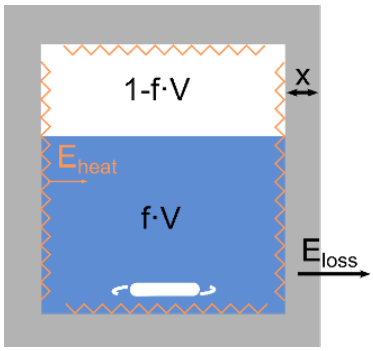

Figure 3S. Schematic of the reactor

Further improvement to our model could be achieved by taking into account the change in volume of the liquid phase with temperature (*i.e.*, allowing for a pressure and temperature dependent heat capacity). However, since the heat capacity of water tends to increase with salt strength and temperature[7], our current model can be considered as an upper limit for the required heating energy.

In **Table 1S**, we compare the energy consumption for precursor production and LFP production via a low temperature hydrothermal synthesis and solid state approach.

	Mass of precursor (kg) needed for 1 kg LFP	Energy (MJ/kg) required for precursor	Energy (MJ/kg) required for LFP
Hydrothermal*			**26.3**
$FeSO_4$	1.23	-	-
H_3PO_4	0.62	12[3]	7.4
LiOH	0.46	41[1]	18.9
Solid State			**21.6**
Li_2CO_3	0.23	41[1]	9.4
Fe_3O_4	0.49	0.72[1]	0.4
$(NH_4)_2HPO_4$	0.84	14[3]	11.8

*The hydrothermal process gives Li_2SO_4 as byproduct.

Table 1S: Mass of precursors needed for LFP synthesis, energy needed for precursor synthesis, and energy needed for LFP synthesis in a hydrothermal and solid state approach.

Thermodynamic constants		
Evaporation enthalpy[6]	$\Delta_v H$	2.26kJ/kg
Heat Capacity liquid phase[6]	C_{liq}^{sp}	4.2kJ/kg
Heat Capacity vapor phase[6]	C_{vap}^{sp}	1.9kJ/kg
Specific density	ρ_{H_2O}	1000kg/m^3
Ambient temperature	T_0	298K
Reaction yield	y	0.95
Pressure[4,5]	$p(T)$	$log_{10}p(T) = \begin{cases} 4.65 - \frac{1440}{T-64.8}, T\epsilon(273,373) \\ 1 \quad\quad\quad\quad\quad, T\epsilon(373,379) \\ 3.56 - \frac{644}{T-198}, T\epsilon(379,479) \end{cases}$
Reactor temperature	T_r	Free variable
Precursor concentration	C_{tot}	Free variable
Reaction time	t	Free variable
Reactor Constants[1]		
Volume	V	10m^3
Surface	A	25m^2
Wall thickness	x	0.1m
Heat transfer coefficient	λ	0.040Wm^{-1}K^{-1}
Heat retention		50%
Heater efficiency	η	0.80

Table 2S: Values and expressions used in the energy consumption analysis.

1. Majeau-Bettez, G.; Hawkins, T. R.; Strømman, A. H., Life Cycle Environmental Assessment of Lithium-Ion and Nickel Metal Hydride Batteries for Plug-In Hybrid and Battery Electric Vehicles. *Environ. Sci. Technol.* **2011**, 45 (10), 4548-4554.

2. Dunn, J. B.; Gaines, L.; Kelly, J. C.; James, C.; Gallagher, K. G., The significance of Li-ion batteries in electric vehicle life-cycle energy and emissions and recycling's role in its reduction. *Energy Environ. Sci.* **2015**, 8 (1), 158-168.

3. Johnson, M. C.; Palou-Rivera, I.; Frank, E. D., Energy consumption during the manufacture of nutrients for algae cultivation. *Algal Research* **2013**, 2 (4), 426-436.

4. Liu, C.-T.; William, T. L. Jr., Vapor pressure of deuterated water from 106 to 300.deg., *J. Chem. Eng. Data* **1970** 15 (4), 510-513

5. Stull, D. R., Vapor Pressure of Pure Substances. Organic and Inorganic Compounds, *Ind. Eng. Chem.* **1947**, 39, 4, 517-540.

6. W. M. Haynes, ed., *CRC Handbook of Chemistry and Physics, 97th Edition (Internet Version 2017)*, CRC Press/Taylor & Francis, Boca Raton, FL.

7. F. D. Rossini, Heat capacities in some aqueous solutions, *J. Res. Natl. Stand.***1930**, 4, 313-335.

D. X-ray diffraction and Rietveld refinement of LFP samples.

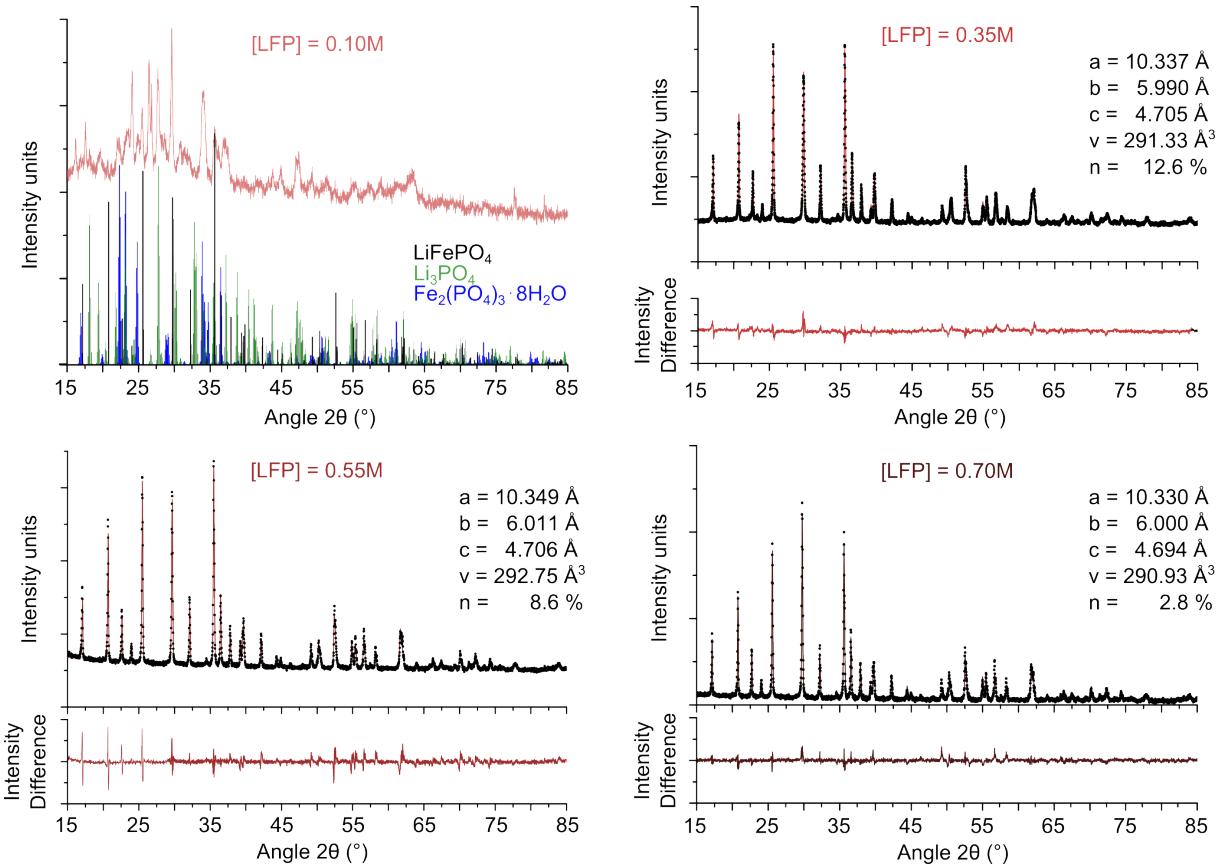

Figure 4S: Rietveld refinement of the XRD spectra of LFP particles synthesized at different precursor concentrations, C_{tot}. For C_{tot}=0.1M, no refinement was possible due to further Li_3PO_4 and $Fe_2(PO_4)_3 \cdot 8H_2O$ impurities. For the other LFP samples, the resulting crystal parameters, the unit cell volume and the antisite defect concentration (n) are given. The difference between refinement and the data is plotted below for each diffractogram.

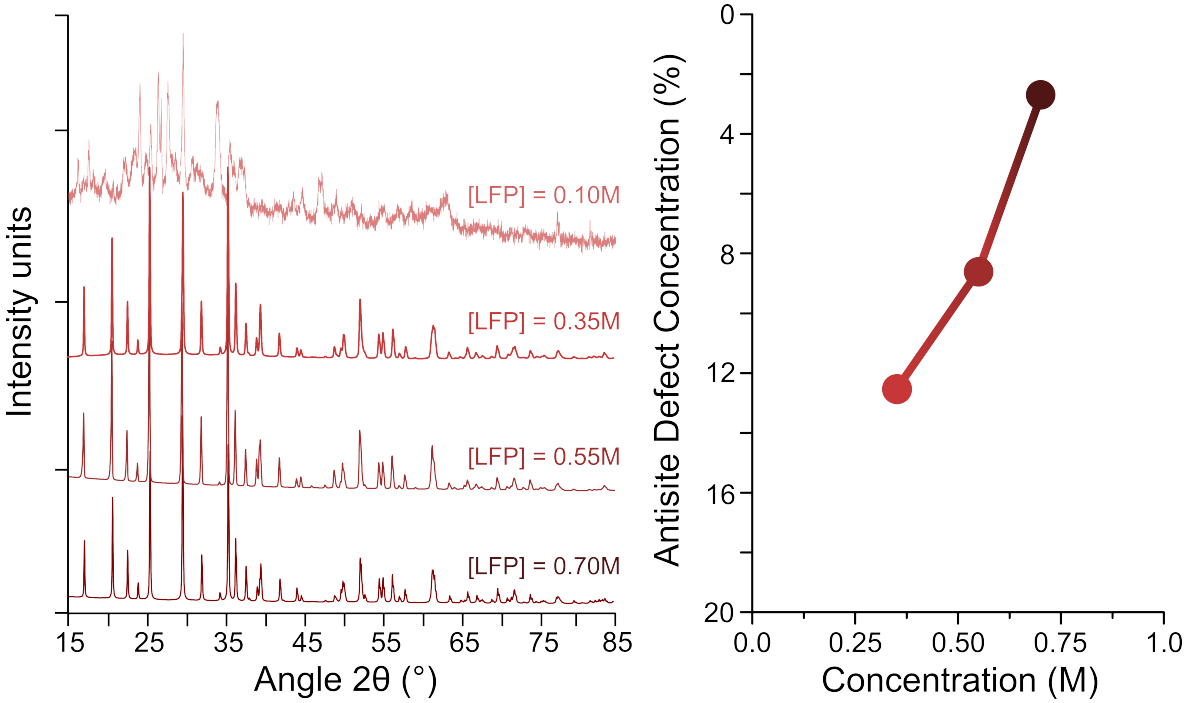

Figure 5S. (a) Comparison of XRD patterns of LFP samples synthesized at different precursor concentrations, C_{tot}. (b) Plot of the resulting antisite defect concentration of the LFP sample as a function of precursor concentration. The antisite defect concentration was obtained from the Rietveld refinements of the LFP data in **Figure 4S**.

E. Sampling Tool.

To take material out of the pressurized reactor, a sampling tool was designed (**Figure 6S**). The sampling unit was designed to fit on our stainless steel reactors. For sampling, a 100 mL reactor size was chosen to ensure that sufficient material remains in the reactor after multiple sampling steps. The LFP product synthesized in the 100 mL reactor with sampling is similar to the material produced in standard 50 mL reactor.

The sampling unit is separated from the reactor with a needle valve. The needle valve remains closed during the reaction except for times when a sample is being taken.

During sampling, material from the reactor automatically enters the sampling unit once the needle valve is opened due to the pressure difference between the reactor and the sampling unit. The valve is closed after a period of time (1 second to 1 minute depending on the pressure difference), trapping material in the sampling unit so that it can then be collected through the tap.

After taking a sample, the sampling unit is cleaned to prevent contamination during subsequent sampling steps. First, the tap is closed and the sampling unit is pressurized via N_2. This causes any remaining material to be pushed back into the reactor when the needle valve is opened. Second, the needle valve is closed, after which, the sampling unit is washed with water and dried with the N_2 stream.

Throughout the reaction, the reactor temperature is monitored with a thermocouple. Material sampling typically results in a temperature change on the order of 1-3°C for at most several minutes. The disturbance of the reaction due to obtaining a sample causes a reduced crystallinity of the platelets visible in the FTIR spectra and a larger error during the particle size measurements. The changes are within the measurement error.

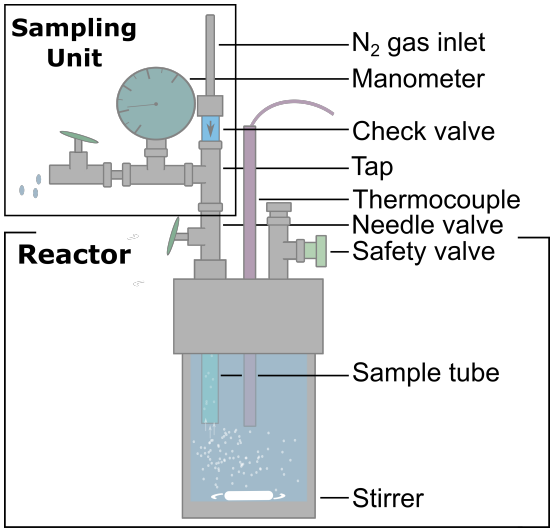

Figure 6S. Schematic of the sampling reactor.

F. Electrochemistry

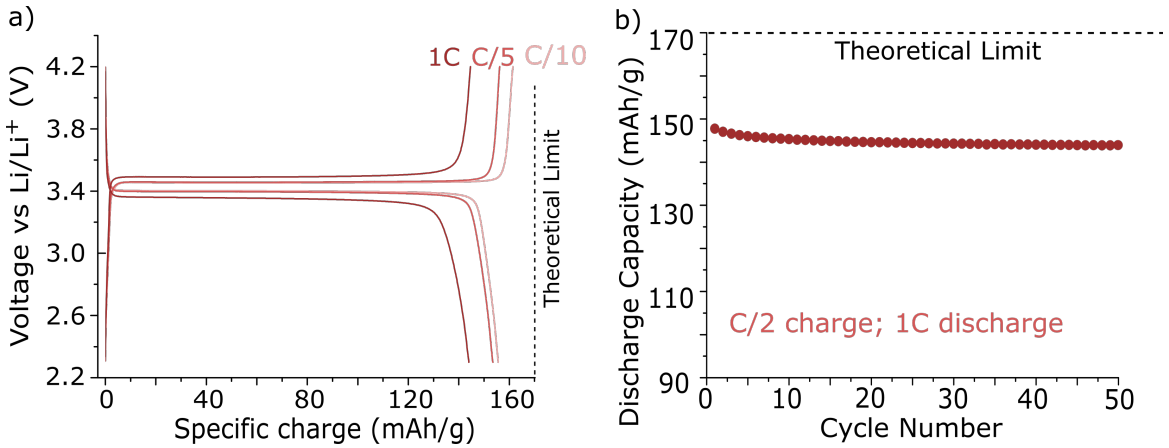

Figure 7S. (a) Galvanostatic curves showing (dis)charge of LFP samples (reaction time: 48 h) at different C-rates. (b) Discharge capacity as a function of cycles measured at 1C discharge and C/2 charge.

G. Time-dependent energy consumption analysis.

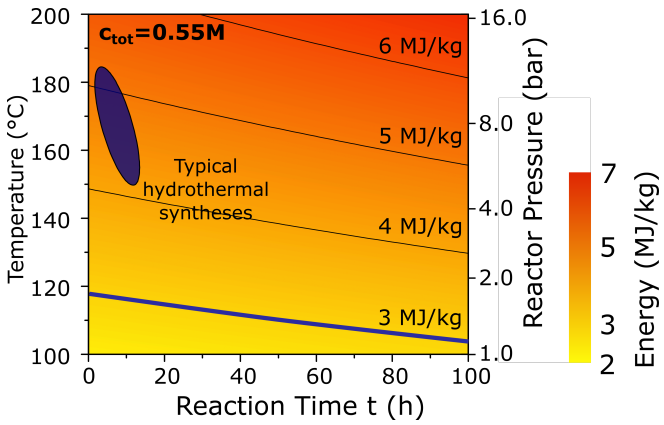

Figure 8S. Specific energy consumption of the LFP synthesis step as a function of hydrothermal reaction temperature (reactor pressure) and reaction time. The energy consumption of typical hydrothermal syntheses of LFP particles is indicated with the blue shading. The 3 MJ/kg energy consumption for a solid state approach is highlighted (blue region and blue line, respectively).